G. BÁNÓ[1],✉
P. HORVÁTH[1]
Z. DONKÓ[1]
K. RÓZSA[1]
T.M. ADAMOWICZ[2]

Sputtered and heated high-voltage hollow-cathode zinc lasers

[1] Research Institute for Solid State Physics and Optics, POB 49, 1525 Budapest, Hungary
[2] Institute of Micro- and Optoelectronics, Warsaw University of Technology, Koszykowa 75, 00-662 Warsaw, Poland

ABSTRACT The operational characteristics of two different high-voltage hollow-cathode zinc ion lasers are reported. The first is a segmented hollow-cathode laser in which the metal vapor is produced by sputtering of the cathode material. In the second, a hollow-anode-cathode laser, the metal is thermally evaporated from a heated side-arm. The small-signal gain on the Zn-II 492.4 nm transition and the multi-line output power on the Zn-II 492.4 and 491.1 nm transitions are measured under different discharge conditions. Small-signal gains of 100 and $60\%\,\mathrm{m}^{-1}$ are obtained with the sputtered and heated lasers, respectively. A comparison of the small-signal gain data with those obtained with other discharge configurations is also presented.

PACS 42.55.Lt; 42.60.Lh; 52.80.-s

1   Introduction

        Zinc and cadmium were the first elements ever used for laser action on transitions of metal ions [1]. In metal ion lasers the upper laser level is usually pumped by charge transfer or Penning ionization of metal atoms during collisions with noble gas ions or metastables, respectively. It follows that metal ion lasers can operate in glow discharges of noble gas-metal mixtures. Different transitions are favorably excited either in the positive column or in the negative glow regions of the discharge [2, 3]. In the latter case various hollow-cathode arrangements can be applied. The metal vapor is then produced by thermal evaporation (heated lasers) or by means of cathode sputtering. For technical reasons, heated hollow-cathode metal ion lasers are only built for metals having low melting temperatures (high vapor pressures), such as cadmium, zinc, or mercury (see e.g. [4–6]). In sputtered systems – utilizing ionic bombardment of the cathode surface – a high enough metal density is easily achieved also for metals with relatively high melting temperatures (gold, copper, silver, or aluminium) (see [7] and the references cited therein). Hollow-cathode lasers are attractive for research because of the numerous ultraviolet metal-ion laser transitions.

Ne-Cu (248.6 nm) and He-Ag (224.3 nm) lasers have recently become commercially available for Raman spectroscopy and fluorescent imaging [8].

        There exists an abundant literature on hollow-cathode zinc lasers. The excitation mechanisms of the laser transitions are summarized in [9]. Lasers with conventional hollow-cathode geometries (cylindrical, slotted, flute-type) have both heated [10–14] and sputtered [15, 16] variants. During the last twenty-five years, several high-voltage hollow-cathode arrangements have been developed (e.g. hollow-anode-cathode [17], helical [18], or segmented hollow-cathode [19]), primarily to increase the efficiency of sputtered systems. Up to now none of these high-voltage constructions have been used as a sputtered zinc laser. In [20–23] the helical hollow-cathode geometry was combined with thermal evaporation of zinc atoms. The zinc laser is attractive because of the possibility of population inversion at the 210 nm Zn-II line in a Ne-Zn discharge. This possibility was suggested first by Collins [24] and has subsequently been studied by Jánossy and Mezei [25]. The 210 nm line would represent the shortest wavelength continuous laser excitation. However, up to now, no definite answer exists on its feasibility.

        In this work we present two novel zinc-ion laser systems: a sputtered segmented hollow-cathode (SHC) laser and a heated hollow-anode-cathode (HAC) laser. Our aim is to examine the operation of the new laser variants and to make a comparison of the zinc laser data available in the literature. We believe that such a comparison can provide information on the different discharge arrangements that are useful not only for the He-Zn lasers but also for the development of other metal-ion laser systems. For both lasers presented here, the measurements are carried out on the Zn-II 492.4 and 491.1 nm transitions excited in a helium buffer gas. As the output power of different lasers depends (besides other factors) on the transmission of the mirrors, we use the small-signal gain data to give some objective (although not complete) comparison between the new and older laser systems.

        The SHC geometry applied in the first laser has previously been proven to be an outstanding pumping source in ultraviolet copper and gold lasers [19, 26, 27]. We have presented some preliminary results obtained with the SHC zinc laser in [28].

        The second laser combines the high-voltage hollow-anode-cathode (HAC) discharge with the thermal evaporation

✉ Fax: +36-1/3922-215, E-mail: bano@sunserv.kfki.hu

of zinc. In this way (in contrast to sputtered lasers), the metal density is independent of the discharge current and both can be optimized at the same time. The applied electrode geometry is chosen on the basis of comparative spectroscopic measurements of different hollow-cathode variants [29]. Our choice of the HAC discharge represents a compromise between the low value of sputtering (not needed in a heated laser) and the high intensity of excited noble-gas-ion transitions.

2 Experimental

2.1 *The sputtered segmented hollow-cathode laser*

The design of the SHC zinc laser is shown in Fig. 1. The discharge region is surrounded by two cathode and two anode surfaces facing each other. Both the cathodes and anodes are made of zinc. The laser tube consists of three SHC discharge modules, each 5 cm long with inner diameter of 4 mm, which are separated by additional anode rings. The outer alumina tube is sealed with epoxy. The measurements are carried out in helium, and small amount of argon is added to the buffer gas to increase the sputtering efficiency.

2.2 *The heated hollow-anode-cathode laser*

The heated HAC laser tube is shown in Fig. 2. The active region consists of six HAC modules, each 6 cm long. Two sets of stainless steel cathodes are investigated, having inner diameters of 12 and 5 mm. The corresponding internal anode systems consist of four anode plates (in the 12 mm diameter tube) and four rods (in the 5 mm diameter tube). The distance between the opposite anode plates (rods) is 4 (2.8) mm. The electrical connections are led through the walls of ceramic tubes towards the flanges at the ends of the outer stainless steel vessel. Zinc is evaporated from a side-arm

placed at the center of the tube. Four separate ovens are used to control the tube temperature. The temperature of the upper parts of the tube is kept about 100 K above the temperature of the side-arm to avoid deposition of the evaporated metal. At the ends of the active region, additional dc positive column discharges are applied as confinement sections to the metal vapor. Due to the cataphoretic effect zinc atoms are selectively driven towards the cathodes, not leaving them to escape from the heated region. This way we eliminate the deposition of the metal in colder parts of the tube, especially on the windows of the laser. The cataphoresis of zinc in helium and neon discharges was studied in detail in [30].

Both lasers operate in the quasi-continuous regime. The discharges are excited with 0.1–1 ms long current pulses at a repetition frequency of 1–5 Hz. External mirrors compose the optical resonator. An output coupler with 0.8% transmission (not optimized) is used for power measurements. The small-signal gain is measured with counter-rotating quartz plates placed in the resonator [31]. This method makes it possible to measure the small-signal gain even below the laser threshold, in the following way. The tube is divided into two parts, an oscillator and an amplifier. First, the losses of the resonator are compensated by the oscillator part bringing the laser to threshold. Next, a certain current is applied to the amplifier, which increases the output power. Finally, the losses are increased by rotation of the quartz plates until threshold operation is re-established. At this point, the gain belonging to the amplifier equals the losses introduced by the plates, which is given by the proper Fresnel formula.

3 Results and discussion

3.1 *The sputtered segmented hollow-cathode laser*

Typical voltage–current characteristics of the SHC discharge obtained in the He + 3%Ar buffer gas are shown
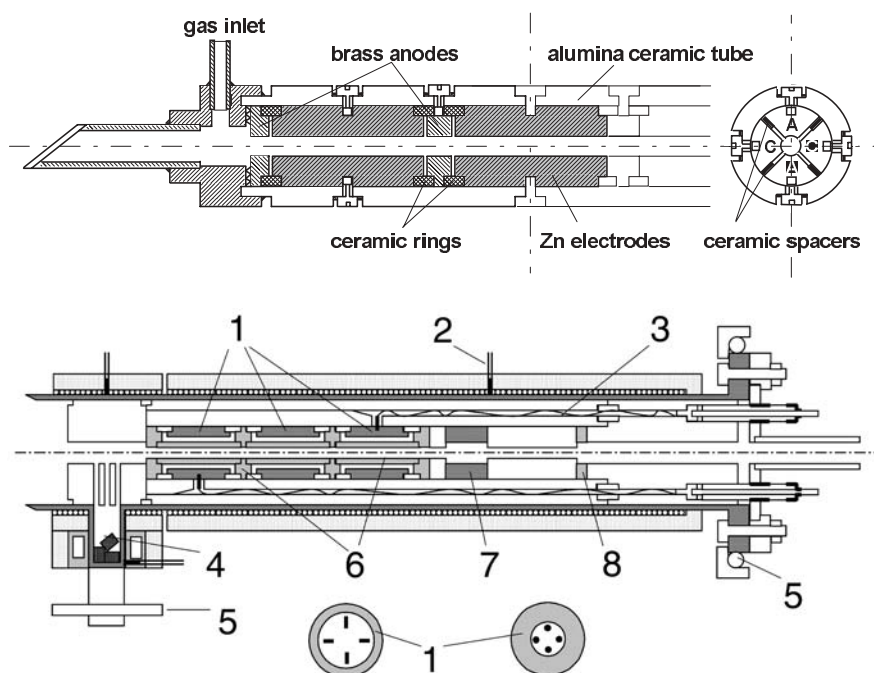

FIGURE 1 The design of the sputtered segmented hollow-cathode zinc laser tube

FIGURE 2 The scheme of the heated hollow anode-cathode zinc laser tube: 1, cathodes; 2, thermocouple; 3, electrical connection; 4, side-arm with zinc pellets; 5, water cooling; 6, internal anode system; 7, 8, the cathode and anode of the positive column cataphoretic confinement section. The cross-section of the 12 and 5 mm diameter cathodes with internal anode plates and rods are also shown

in Fig. 3. The high slope resistance, which is characteristic for high-voltage hollow-cathode configurations, increases the stability of the discharge [32]. At typical conditions the voltage decreases towards higher pressures.

The effect of the argon admixture on the operation of SHC discharges has been studied in more detail in connection with the gold laser [27]. In the present work the optimal argon admixture concentration for laser operation was obtained by measuring the dependence of the laser threshold current on the argon concentration (see Fig. 4). This way the optimal discharge conditions were determined to be 3% of argon in the helium buffer gas at a pressure of 8 mbar.
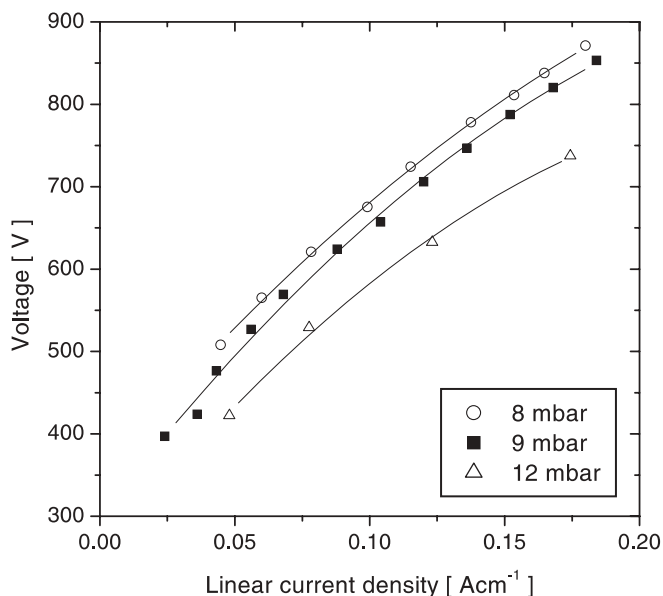
The multi-line output power at a current of 1.75 A (the active length is 15 cm) and optimal discharge conditions is 10 mW.

3.2 *The heated hollow-anode-cathode laser*

The voltage–current characteristics of the 12 mm inner diameter HAC tube are shown in Fig. 5. Adding zinc vapor to the helium discharge, the ionic current is carried both by helium and zinc ions. In spite of the lower ionization potential of zinc atoms (compared with helium) the

FIGURE 3   Voltage–current characteristics of the segmented hollow-cathode discharge at different pressures of the He + 3%Ar buffer gas
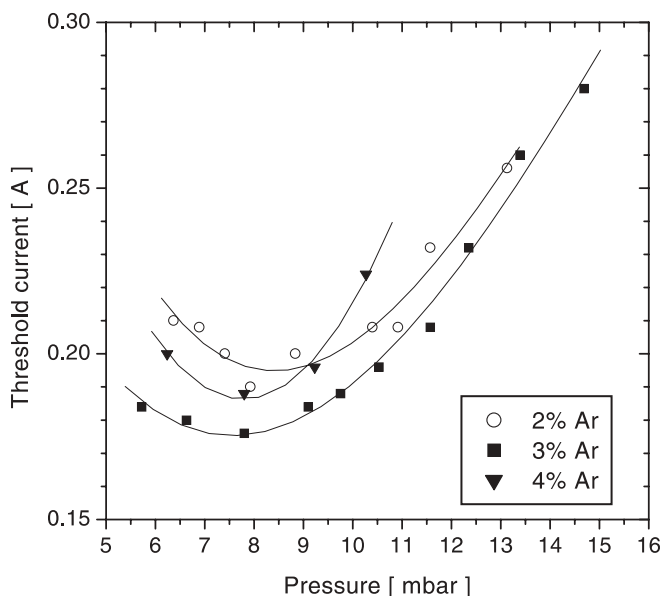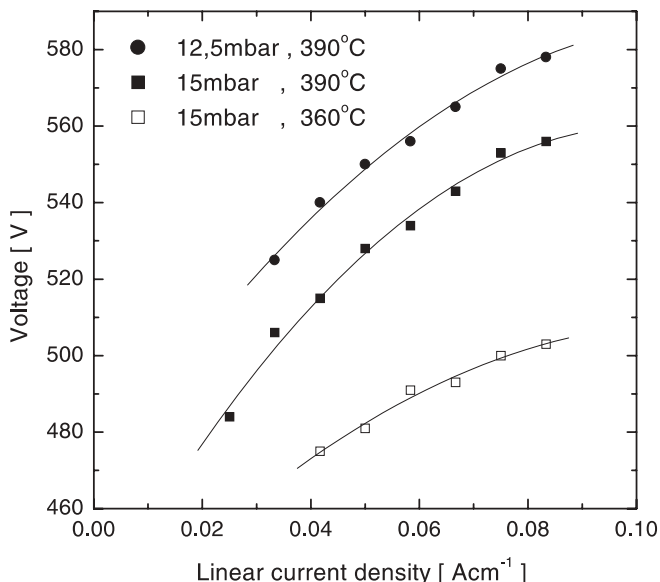
FIGURE 4   Threshold current of the 492.4 nm segmented hollow-cathode laser as a function of pressure at different percentages of argon added to the helum buffer gas

FIGURE 5   Voltage–current characteristics of the 12 mm inner diameter hollow-anode-cathode discharge at different buffer gas pressures and side-arm temperatures
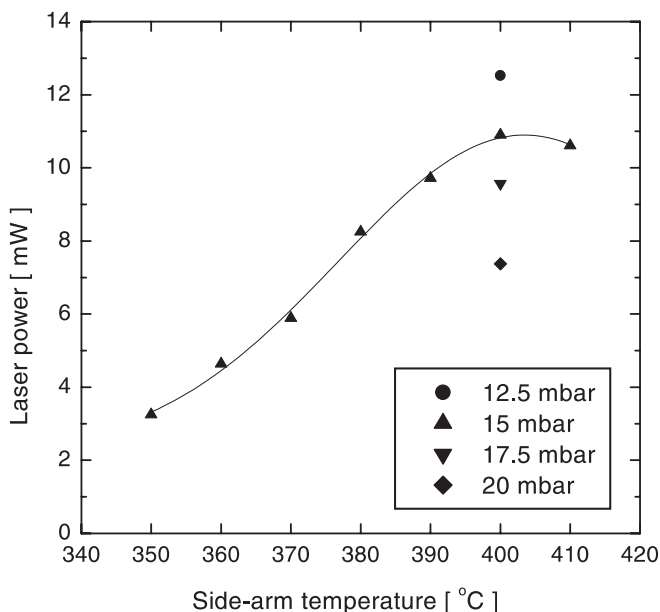
FIGURE 6   Multi-line laser output power of the 12 mm inner diameter hollow-anode-cathode laser on the two blue transitions as a function of the side-arm temperature. The linear current density is 0.08 A cm^{-1} and the active length is 36 cm. The resonator consists of 0 and 0.8% transmission mirrors

voltage increases with the density of metal vapor. This result can be explained by the lower electron emission coefficients of metal ions impinging on the cathode surface. The higher voltage compensates for the lower yield of liberated electrons.

The multi-line output power on the Zn-II 492.4 and 491.1 nm transitions is depicted in Fig. 6 as a function of the side-arm temperature. In agreement with earlier results [22] the highest output power is achieved at a zinc vapor density that corresponds to a side-arm temperature of 400 °C. Towards higher zinc concentrations the density of helium ions decreases, which is reflected in the decrease of the laser power above 400 °C. The pressure dependence belonging to the optimal temperature can also be seen in Fig. 6. Because of the large cathode diameter (12 mm) the optimal pressure is lower than 10 mbar. However, as the pressure decreases the efficiency of the cathaphoretic confinement section becomes worse, due to the easier diffusion of metal atoms (see [30]). This limitation prevents us from operating the laser below 10 mbar.

3.3 *Small-signal gain coefficient at* 492.4 nm

As the small-signal gain coefficient of the blue laser is measured in the laser operated at threshold (at threshold currents) and as no wavelength selection is applied, our data belong to the stronger, 492.4 nm transition. Results obtained at optimal discharge conditions are shown in Fig. 7, together with other data accessible from the literature. The results are plotted as a function of linear current density.
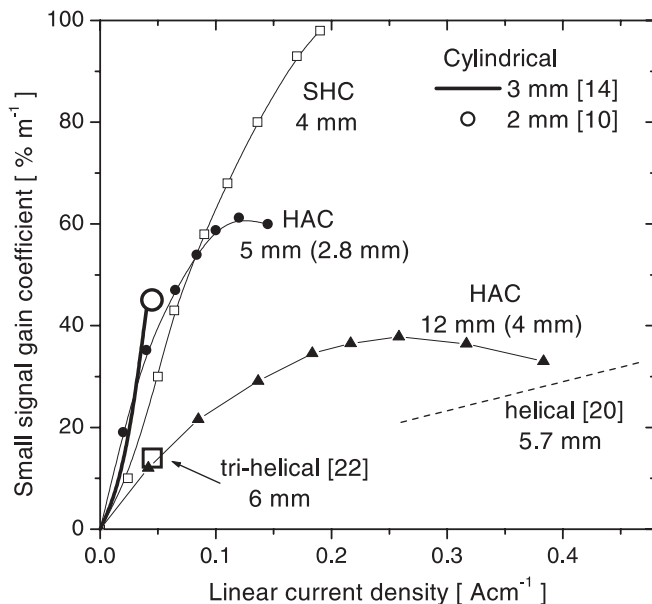

FIGURE 7 Current dependence of the small-signal gain coefficient on the 492.4 nm transition. Results of the present SHC and HAC measurements are shown together with other data available in the literature. The inner diameters of the cathodes (and the internal diameter of the HAC anode system) are indicated. The following discharge conditions belong to present data: SHC – 8.7 mbar of He + 3%Ar buffer gas; 12 mm HAC – 12.7 mbar and side-arm temperature of 390 K; 5 mm HAC–18 mbar and side-arm temperature of 400 K

The highest small-signal gain coefficient (100% m^{-1}) is obtained with the sputtered SHC laser tube, showing the advantageous features of the segmented discharge. Unfortunately, due to the high current densities, the sputtering of zinc cathodes was very strong and the deposited metal created short circuits between the cathodes and anodes, thus seriously limiting the laser's lifetime. It is noted that the formation of short circuits was not a serious problem while using the SHC arrangement for excitation of a gold laser [27]. To solve the problem in the future we plan to increase the distance between the electrode edges by using rounded anode electrodes. Preliminary measurements on an infrared copper laser indicate that such a modification results in only a 30% decrease of the laser power.

In the heated HAC laser the cathode is made of stainless steel to minimize the sputtering of the cathode material. There is a significant difference between the gain coefficients using 12 and 5 mm inner diameter HAC discharges. High gain values are reached at much lower currents in the narrow tube. The same behavior was reported for the laser power in heated cylindrical discharges [11]. Comparing all the data in Fig. 7 we conclude that it is advantageous to use smaller diameter discharges to reach high gain values. It can also be seen that at lower current densities the gain obtained with conventional cylindrical discharges is approximately the same as that of our 5 mm inner diameter HAC laser tube. The advantage of the cylindrical arrangement is the simpler construction. However, using the HAC arrangement stable discharge operation can be obtained at higher current densities. This is due to the high slope resistance of the high-voltage HAC discharge.

Using both the 12 and 5 mm inner diameter HAC tubes the gain passes over a maximum and starts to decrease above a given current density. Piper and Gill proposed in [11] that there may be a starvation of neutral zinc in the discharge volume at high current densities due to the 'imprisonment' of large fraction of the metal as ground-state metal ions. Based on the calculations given in [27] for the sputtered segmented hollow-cathode gold laser or in [33] for a heated cylindrical hollow-cathode mercury laser, we can roughly estimate the ionic density at the tube center to be about 1×10^{14} cm^{-3} for a linear current density of 0.1 A cm^{-1}. Assuming that the majority of the positive charge is carried by zinc ions [33] the zinc ion density is found to be only one-tenth of the density of zinc atoms (1×10^{15} cm^{-3} for a side-arm temperature of 400 °C). However, as zinc ions are mostly created in the central region of the discharge one has to consider the radial ionic flux (towards the walls, where the ions recombine) due to ambipolar diffusion. At equilibrium conditions this radial flux of ions has to be compensated by an opposite flux of metal atoms towards the tube center. Since the ions diffuse approximately four times faster compared with neutral zinc atoms, a significant dip may occur in the radial distribution of neutral metal atoms at the tube center. The increasing depth of this minimum towards higher currents may cause the turn-over of the laser gain values. Another possible mechanism is that, at high current densities, direct electron excitation of the lower laser level becomes significant, resulting in the decrease of the small-signal gain (see also [34]).

4   Conclusions

The characteristics of zinc ion lasers operating on the 492.4 and 491.1 nm transitions in a sputtered SHC and a heated HAC laser tube have been compared. To our best knowledge the small-signal gain coefficient of 100% m^{-1} obtained with the SHC tube is the highest ever reported for the 492.4 nm line. Moreover, the sputtered SHC laser is significantly easier to operate than the heated one. Based on the experience that we gained during the measurements, we conclude that the SHC arrangements needs to be modified for use as a practical zinc or other metal-ion laser. A modified electrode arrangement and a high-purity construction are needed to prevent the formation of short circuits and to ensure reasonable lifetimes.

The highest gain obtained with the heated HAC tube was 60% m^{-1}. We have shown that, in general, it is advantageous to use smaller cathode-diameter discharges for zinc lasers. It is not obvious which heated arrangement is the best candidate for a practical laser design. One has to take into account both construction and discharge stability considerations.

REFERENCES

1 G.R. Fowles, W.T. Silfvast: IEEE J. Quantum Electron. **QE-1**, 131 (1965)
2 P. Gill, C.E. Webb: J. Phys. D: Appl. Phys. **10**, 299 (1976)
3 P. Gill, C.E. Webb: J. Phys. D: Appl. Phys. **10**, 2235 (1977)
4 W.K. Schuebel: Appl. Phys. Lett. **16**, 470 (1970)
5 Y. Sugawara, V. Tokiwa: Jpn. J. Appl. Phys. **9**, 588 (1970)
6 J.A. Piper, C.E. Webb: Opt. Commun. **13**, 122 (1975)
7 D.C. Gerstenberger, R. Solanki, G.J. Collins: IEEE J. Quantum Electron. **QE-16**, 820 (1980)
8 M.C. Storrie-Lombardi, W.F. Hug, G.D. McDonald, A.I. Tsapin, K.H. Nealson: Rev. Sci. Instrum. **72**, 4452 (2001)
9 G.J. Collins: J. Appl. Phys. **44**, 4633 (1973)
10 H. Tsuda, J.A. Piper: J. Phys. E: Sci. Instrum. **22**, 462 (1989)
11 J.A. Piper, P. Gill: J. Phys. D: Appl. Phys. **8**, 127 (1975)
12 T. Iijima, Y. Sugawara: J. Appl. Phys. **45**, 5091 (1974)
13 R.C. Jensen, G.J. Collins, W.R. Bennett: Appl. Phys. Lett. **18**, 50 (1971)
14 P. Gill, J.A. Piper: Opt. Commun. **22**, 288 (1977)
15 M. Jánossy, P. Mezei: Appl. Phys. B **66**, 47 (1998)
16 E.K. Karabut, W.S. Mikhalevskii, V.F. Papkin, M.F. Sem: Sov. Phys. Tech. Phys. **14**, 1447 (1970)
17 K. Rózsa, M. Jánossy, L. Csillag, J. Bergou: Opt. Commun. **23**, 162 (1977)
18 M. Grozeva, N. Sabotinov: Opt. Commun. **41**, 57 (1982)
19 Z. Donkó, L. Szalai, K. Rózsa, M. Ulbel, M. Pockl: IEEE J. Quantum Electron. **QE-34**, 47 (1994)
20 M.S. Stefanova, P.M. Pramatarov, A.A. Peeva: Proc. SPIE **3571**, 150 (1999)
21 A.A. Peeva, P.M. Pramatarov, M.S. Stefanova: Proc. SPIE **3571**, 154 (1999)
22 M. Stefanova, P. Pramatarov: Phys. Lett. A **139**, 391 (1989)
23 V. Derzhiev, A. Karelin, O. Sereda, M. Stefanova, S. Yakovlenko: Appl. Phys. B, **51**, 465 (1990)
24 G.J. Collins: Thesis, Yale University, New Haven, USA (1970)
25 M. Jánossy, P. Mezei: Z. Naturforsch. **53a**, 955 (1998)
26 K.A. Peard, R.C. Tobin, K. Rózsa, Z. Donkó: IEEE J. Quantum Electron. **QE-30**, 1181 (1994)
27 G. Bánó, L. Szalai, K. Kutasi, Z. Donkó, K. Rózsa, T.M. Adamowicz: J. Appl. Phys. **92**, 6372 (2002)
28 T.M. Adamowicz, G. Bánó, L. Szalai, K. Dzieciolowski, W. Kwasniewski, Z. Donkó, K. Rózsa: In: 11th Symp. Elementary Processes and Chemical Reactions in Low Temperature Plasmas, in Low Tatras, 22–26 June 1998, book of contributed papers, p. 11
29 P. Horváth, G. Bánó, K. Rózsa: In: XVth ESCAMPIG in Lillafured, Hungary, 26–29 August 2000. Europhys. Conf. Abstr. **24F**, 476 (2000)
30 G. Bánó, P. Horváth, K. Rózsa: J. Phys. D: Appl. Phys. **33**, 2611 (2000)
31 K.A. Peard, R.C. Tobin, K. Rózsa, Z. Donkó: IEEE J. Quantum Electron. **QE-30**, 1181 (1994)
32 K. Rózsa: Z. Naturforsch. **35a**, 649 (1980)
33 G.J. Fetzer, J.J. Rocca: IEEE J. Quantum Electron. **QE-28**, 1941, (1992)
34 K. Jain, S.A. Newton: Appl. Phys. B **26**, 43 (1981)